Available online at www.sciencedirect.com
SCIENCE DIRECT®
ELSEVIER
International Journal of Multiphase Flow 30 (2004) 273–290
International Journal of Multiphase Flow
www.elsevier.com/locate/ijmulflow

Modelling of gas entrainment from Taylor bubbles. Part B: A stationary bubble

N. Brauner *, A. Ullmann

Department of Fluid Mechanics and Heat Transfer, Faculty of Engineering, Tel Aviv University, Tel Aviv 69978, Israel

Received 1 September 2002; received in revised form 24 November 2003

Abstract

The model presented in Part A of this study is revised for the case of gas entrainment from a stationary bubble injected into liquid down-flow. Comparisons with data available from the literature substantiate the model as a quantitative predictive tool for the effects of bubble length, physical properties of fluids, tube diameter and inclination on the rate of gas entrainment from stationary large bubbles.

The similarity and differences between the fragmentation of a stationary bubble and an upward rising free bubble are discussed. It is shown that data obtained with a stationary bubble in liquid down-flow may display smaller gas entrainment rate from a similar upward rising Taylor bubble and therefore, may underestimate the aeration of the liquid bridge in slug flow.

Keywords: Air entrainment; Down-flow; Elongated bubble; Fragmentation; Gas–liquid; Slug flow

1. Introduction

The interest in gas entrainment from stationary large bubbles attached to spargers emerges from two diverse routes. One is related to the design and performance of circulating bubble columns, such as air-lift reactors and fermenters. The other is to get insight into the air entrainment process from the Taylor bubbles in gas–liquid slug flow. In real slug flow, measurements of the gas entrainment into the liquid slug are complicated due to the fast movement of the Taylor bubbles and the intermittency in the flow.

* Corresponding author. Tel.: +972-3-6408127/8930; fax +972-3-6407334.
E-mail address: brauner@eng.tau.ac.il (N. Brauner).

0301-9322/$ - see front matter
doi:10.1016/j.ijmultiphaseflow.2003.11.008

Experimental studies on gas entrainment from a stationary bubble are reported in the literature. A gas cavity of the shape of an elongated (Taylor) bubble (EB) is obtained by a controlled injection of gas into liquid down-flow in a pipe (e.g. Riiser et al., 1992; Bacon et al., 1995a,b; Lee et al., 1997; Delfos et al., 2001a,b; Hernandez-Gomez and Fabre, 2001). With increasing the gas injection rate, the length of the EB increases, until the rate of bubble entrainment at the EB tail is balanced by the rate of gas injection. However, when the gas injection rate exceeds the maximal bubble entrainment rate, unbounded EB growth is encountered. Therefore, in case the EB stabilizes at a constant length, the measured gas injection rate corresponds to the rate of bubble entrainment. Bacon et al. (1995a,b) studied the effects of the sparger design, liquid flow rate and physical properties, and the EB length on the bubble entrainment rate in a vertical pipe. The studies were extended by Lee et al. (1997, 1999) focusing on the issue of diameter scale-up by using a larger diameter column. Based on the collected data, a dimensionless correlation for the maximal gas entrainment rate has been suggested, which essentially indicate that the gas Froude number is dependent on the liquid Froude number and the system Eötvös number. The correlation parameters, however, are found to be dependent on the type of sparger used.

The studies of Delfos et al. (2001a) and Hernandez-Gomez and Fabre (2001) represent attempts to simulate slug flow in a vertical pipe and 30° inclined pipe, respectively. In these studies, special attention has been paid to mimic the shape of the elongated bubble nose and the relative velocities of the liquid and the EB in slug flow.

Basically, all these experimental studies indicate that the EB fragmentation is related to the liquid film velocity as it plunges into the liquid column beneath the EB. However, a quantitative model that can explain the experimentally observed phenomena, has not been developed heretofore.

In Part A of this study (Brauner and Ullmann, 2004), a physical model for the entrainment of bubbles from the Taylor bubble tail in slug flow, the Taylor bubble wake (TBW) model, has been developed. The fragmentation of the Taylor bubble (TB) has been attributed to the turbulence in the wall jet and shear layer, which are formed in the Taylor bubble wake, as the liquid film plunges into the liquid slug. The rate of gas entrainment has been determined based on an energy balance between the rate of turbulent kinetic energy generated and the rate of bubble surface energy production. The model has been tested against experimental data available from the literature on slug flow. It is shown to predict the effects of liquid and gas flow rates and physical properties, as well as the effects of tube diameter and inclination on the void fraction in the liquid slug and associated phenomena in slug flow. In this study, the TBW model is revised for the case of bubble entrainment from a stationary EB. The model predictions are compared with available experimental data.

2. The Taylor bubble wake (TBW) model for a stationary bubble

The underlying physical mechanism for fragmentation of the elongated bubble (EB) and gas entrainment into the liquid are elucidated in view of Fig. 1a for vertical flow and Fig. 1b for inclined flow. Gas is injected at a flux U_{GS} to form a single stationary EB in downward liquid flow of a flux U_{LS}. If fragmentation of the EB does not take place, the EB expands in the downstream direction at a rate $U_{GB}^{w} = U_{GS}/\varepsilon_{B}^{w}$, where ε_{B}^{w} is the local void fraction at the EB tail. However, the

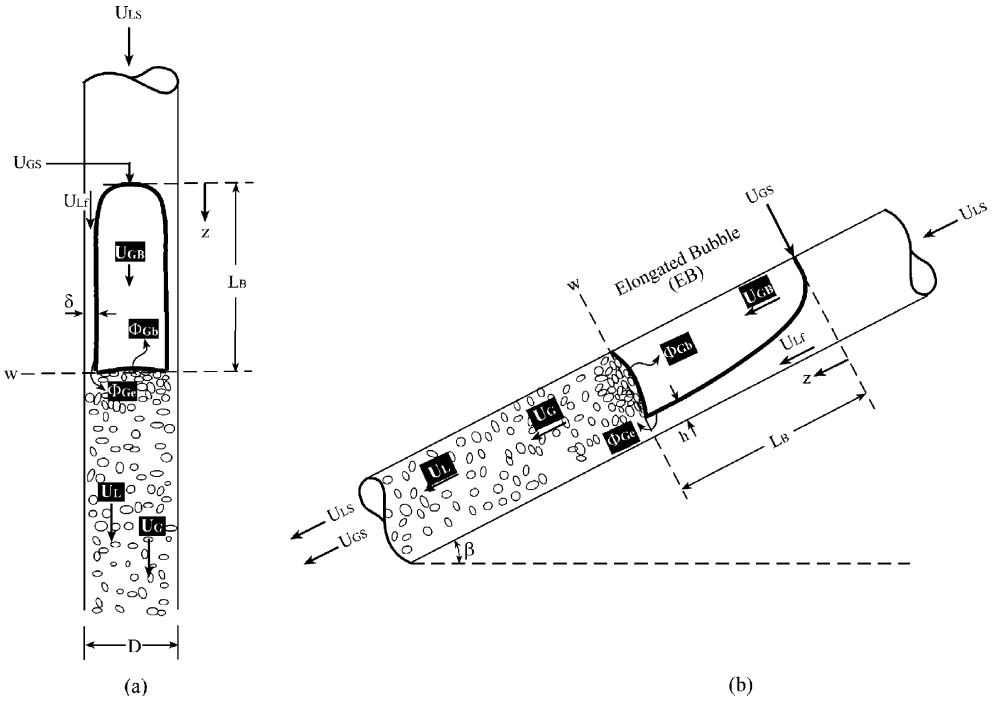

Fig. 1. Schematic description of the physical model for a stationary elongated bubble in liquid down-flow: (a) a vertical tube, (b) an inclined tube.

liquid film formed around the EB plunges into the liquid column below the EB. This results in fragmentation of the EB tail and entrainment of small bubbles into its wake at a rate Φ_{Ge}. Part of the entrained bubbles may re-coalesce with the EB tail (at a rate Φ_{Gb}), resulting in a net gas rate of $\Phi_{GS} = \Phi_{Ge} - \Phi_{Gb}$, which is carried downward as bubbly flow. The EB length, L_B stabilizes when the net rate of bubble entrainment at its tail Φ_{GS} is equal to the rate of gas injection into the EB at its nose, U_{GS}.

The flow phenomena as observed in the TB wake region is non-stationary, highly disordered and involve sequence of events of the tail expansion followed by its fragmentation. Typically, the in situ void fraction in the EB wake region, ε_L^w can be higher than the in situ void fraction downstream in the EB far wake region, ε_L^s.

The rate of gas entrainment from the EB tail is determined based on an energy balance between the flux of turbulent kinetic energy generated at the EB wake and the flux of bubble surface energy production. The turbulent model for characterizing the eddy velocity components (u', v', w') and the dispersive forces is that associated with a wall jet and shear layer formed at the EB wake due to the relative velocity between the liquid bulk (moving at a velocity U_L^w) and the plunging liquid film of a velocity U_{Lf}^w.

Experimental studies by Bacon et al. (1995a,b), Hernandez-Gomez and Fabre (2001) and Delfos et al. (2001a) indicate that gas entrainment is initiated when the bubble length exceeds a certain threshold value. Shorter EB's, once formed, can be maintained without continuous gas

supply. In Part A of this study (Brauner and Ullmann, 2004) the onset of entrainment has been related to a critical Weber number:

$$We'_{\mathrm{crit}} = \frac{\rho_{\mathrm{L}} d_{\max}(u'^2 + v'^2 + w'^2)_{\mathrm{crit}}}{3\sigma} = C' \simeq \mathrm{O}(1); \quad (u'^2 + u'^2 + w'^2)_{\mathrm{crit}} \simeq 0.03(U_{\mathrm{Lf}}^{\mathrm{w}} - U_{\mathrm{L}}^{\mathrm{w}})^2_{\mathrm{crit}} \quad (1)$$

The expression obtained for the flux of gas due to fragmentation of the EB trail is given by

$$\frac{\Phi_{\mathrm{Ge}}}{\Phi_{\mathrm{Lf}}} = \frac{1}{400 C_J} \tilde{d}_{\mathrm{crit}}(We - We_{\mathrm{c}}); \quad We \geqslant We_{\mathrm{c}} \tag{2.1}$$

$$We = \frac{\rho_{\mathrm{L}} D(U_{\mathrm{Lf}}^{\mathrm{w}} - U_{\mathrm{L}}^{\mathrm{w}})^2}{\sigma}; \quad We_{\mathrm{c}} = \frac{100 C'}{\tilde{d}_{\mathrm{crit}}} \tag{2.2}$$

where the characteristic maximal bubble size was taken as the critical size of deformable bubbles, d_{crit}:

$$\tilde{d}_{\mathrm{crit}} = \frac{d_{\mathrm{crit}}}{D} = \left[\frac{0.4\sigma}{(\rho_{\mathrm{L}} - \rho_{\mathrm{G}}) g \cos\beta' D^2}\right]^{1/2} = \frac{0.224}{(\cos\beta' Eo_D)^{1/2}}; \quad Eo_D \geqslant 0.2 \tag{3.1}$$

$$\tilde{d}_{\mathrm{crit}} = 0.25; \quad Eo_D < 0.2$$

$$Eo_D = \frac{\Delta\rho g D^2}{8\sigma}; \quad \beta' = \begin{cases} |\beta|; & |\beta| \leqslant 45^\circ \\ 90 - |\beta|; & |\beta| > 45^\circ \end{cases} \tag{3.2}$$

and

$$\Phi_{\mathrm{Lf}} = (U_{\mathrm{Lf}}^{\mathrm{w}} - U_{\mathrm{GB}}^{\mathrm{w}})(1 - \varepsilon_{\mathrm{B}}^{\mathrm{w}}) \tag{4}$$

C_J and C' are tunable constants of the order of 1 ($C_J = 1$, $C' = 0.6$ are used here).

The bubbly flow in the slug region is described by the drift flux model. The bubbles and liquid velocities in the EB wake, $U_{\mathrm{G}}^{\mathrm{w}}$ and $U_{\mathrm{L}}^{\mathrm{w}}$ are given by

$$U_{\mathrm{G}}^{\mathrm{w}} = C_0^{\mathrm{w}} U_{\mathrm{m}} - U_0^{\mathrm{w}}; \quad U_{\mathrm{m}} = U_{\mathrm{LS}} + \Phi_{\mathrm{GS}} \tag{5.1}$$

$$U_{\mathrm{L}}^{\mathrm{w}} = \frac{U_{\mathrm{m}} - \varepsilon_{\mathrm{L}}^{\mathrm{w}} U_{\mathrm{G}}^{\mathrm{w}}}{(1 - \varepsilon_{\mathrm{L}}^{\mathrm{w}})} \tag{5.2}$$

$$U_0^{\mathrm{w}} = 1.53\left[\frac{\sigma g(\rho_{\mathrm{L}} - \rho_{\mathrm{G}})}{\rho_{\mathrm{L}}^2}\right]^{0.25} \sin\beta (1 - \varepsilon_{\mathrm{L}}^{\mathrm{w}})^{1.5} \tag{5.3}$$

where C_0^{w} represents the distribution parameter, which accounts for the bubble concentration and velocity profiles in the EB wake, and U_0^{w} is the bubble drift velocity. Downstream the EB wake region, the liquid and gas velocities $U_{\mathrm{L}}^{\mathrm{s}}$ and $U_{\mathrm{G}}^{\mathrm{s}}$ are obtained using Eqs. (5) with superscript 's' replacing superscript 'w' everywhere.

Part of the bubbles that are entrained from the EB may re-coalesce with its tail. Similar reasoning that led to the estimation of the back-flow to the Taylor bubble in Part A (Brauner and Ullmann, 2004) is applied here. Although the average bubble back-flow may be also a result of the instantaneous velocity components, the bubble back-flow is estimated here based on relative velocity between the drift velocity of the entrained bubbles and the gas velocity at the EB tail, assuming the fluid at the EB tail is stagnant:

$$\Phi_{\mathrm{Gb}} = (U_0^{\mathrm{w}} + U_{\mathrm{GB}}^{\mathrm{w}})\varepsilon_{\mathrm{L}}^{\mathrm{w}}\varepsilon_{\mathrm{B}}^{\mathrm{w}} \tag{6}$$

The net rate of gas loss due to bubble entrainment into the liquid flow is therefore:

$$\Phi_{\mathrm{GS}} = \begin{cases} \Phi_{\mathrm{Ge}} - \Phi_{\mathrm{Gb}} & \Phi_{\mathrm{Ge}} > \Phi_{\mathrm{Gb}} \\ 0 & \Phi_{\mathrm{Ge}} \leqslant \Phi_{\mathrm{Gb}} \end{cases} \tag{7}$$

For maintaining a constant EB length, the net flux of entrained gas equals the gas supply:

$$U_{\mathrm{GS}} = \Phi_{\mathrm{GS}} \tag{8}$$

Otherwise, for $U_{\mathrm{GS}} > \Phi_{\mathrm{GS}}$, the bubble length increases and eventually unbounded bubble growth ('bubble runaway') is encountered.

The in situ gas holdup in the EB wake region and in the liquid downstream are given by

$$\varepsilon_{\mathrm{L}}^{\mathrm{w}} = \frac{\Phi_{\mathrm{GS}}}{U_{\mathrm{G}}^{\mathrm{w}}} \tag{9.1}$$

$$\varepsilon_{\mathrm{L}}^{\mathrm{s}} = \frac{\Phi_{\mathrm{GS}}}{U_{\mathrm{G}}^{\mathrm{s}}} \tag{9.2}$$

Higher void fraction in the wake, $\varepsilon_{\mathrm{L}}^{\mathrm{w}} > \varepsilon_{\mathrm{L}}^{\mathrm{s}}$, can result in case $U_{\mathrm{G}}^{\mathrm{w}} < U_{\mathrm{G}}^{\mathrm{s}}$. In view of Eq. (5.1) it implies $C_0^{\mathrm{w}} < C_0^{\mathrm{s}}$ as a result of the different velocity profiles and bubble radial distributions in the wake region and further downstream. It is worth noting that for non-negligible slip between the liquid and the entrained bubbles, $U_{\mathrm{G}}^{\mathrm{w}}$, $U_{\mathrm{G}}^{\mathrm{s}}$ depend on the in situ void fraction. Therefore, Eqs. (9) are implicit equations for the unknown void fraction.

The equation for the gas entrainment rate, Φ_{Ge} requires the value of the film velocity. The holdup of the liquid film, the film flow rate and the average velocity vary with the distance from the EB nose, $\tilde{z} = z/D$ (see Fig. 1). The in situ holdup, as a function of the position along the EB, is determined by solving the momentum equation on the liquid film. The interfacial shear stress and the inertia of the gas flow in the bubble are found to have a negligible effect and therefore ignored. This way, the calculation of the film thickness profile is decoupled from the unknown gas flux, which would stabilize the EB at a specified length. For liquid flowing in an annular configuration (as in a vertical column) the gradient of the liquid film holdup is given by

$$\frac{\mathrm{d}\varepsilon_{\mathrm{f}}}{\mathrm{d}\tilde{z}} = -\frac{\mathrm{d}\varepsilon_{\mathrm{B}}}{\mathrm{d}\tilde{z}} = -\frac{D\Delta\rho g\sin\beta - \frac{4\tau_{\mathrm{f}}}{\varepsilon_{\mathrm{f}}}}{\rho_{\mathrm{L}}\frac{U_{\mathrm{Lf}}^2}{\varepsilon_{\mathrm{f}}}}; \quad \varepsilon_{\mathrm{f}} = 1 \text{ at } \tilde{z} = 0 \tag{10.1}$$

where

$$\tilde{z} = z/D \quad \tilde{\delta} = \delta/D \quad \text{and} \quad \varepsilon_{\mathrm{f}} = 4\tilde{\delta}(1-\tilde{\delta}) = 1 - \varepsilon_{\mathrm{B}} \tag{10.2}$$

It is important to point out that the one-dimensional momentum balance used to model the variation of the film thickness, Eq. (10.1) breaks down in case the film thickness gradient is not small enough. Therefore, results obtained with a short EB ($\sim 1D$) should be considered only as a rough approximation.

For liquid flowing in a stratified configuration, as in horizontal and inclined column, the dimensionless layer thickness is denoted by $\tilde{h} = h/D$ and the gradient of the liquid holdup is given by

$$\frac{\mathrm{d}\varepsilon_{\mathrm{f}}}{\mathrm{d}\tilde{z}}=\frac{4}{\pi}\widetilde{S}_i\frac{\mathrm{d}\tilde{h}}{\mathrm{d}\tilde{z}}=\frac{4}{\pi}\frac{\frac{\pi}{4}D\Delta\rho g\sin\beta-\frac{\tau_{\mathrm{f}}\widetilde{S}_{\mathrm{f}}}{\varepsilon_{\mathrm{f}}}}{\frac{\pi D\Delta\rho g\cos\beta}{4\widetilde{S}_i}-\rho_{\mathrm{L}}\frac{U_{\mathrm{Lf}}^2}{\varepsilon_{\mathrm{f}}}};\quad \varepsilon_{\mathrm{f}}=\varepsilon_{\mathrm{fc}}\ \text{at}\ \tilde{z}=0 \tag{11.1}$$

where

$$\widetilde{S}_i=\sqrt{1-(2\tilde{h}-1)^2};\quad \widetilde{S}_{\mathrm{f}}=\pi-\cos^{-1}(2\tilde{h}-1) \tag{11.2}$$

The value of $\varepsilon_{\mathrm{fc}}$, used as boundary conditions in Eq. (11.1), corresponds to the critical liquid holdup where $\mathrm{d}\varepsilon_{\mathrm{f}}/\mathrm{d}\tilde{z}\to\infty$ (i.e., the value of ε_{f} where the denominator of the r.h.s. of (11.1) vanishes). The local average velocity in the liquid film and the wall shear stress are given by

$$U_{\mathrm{Lf}}=\frac{U_{\mathrm{LS}}}{\varepsilon_{\mathrm{f}}};\quad \tau_{\mathrm{f}}=\frac{1}{2}f_{\mathrm{f}}\rho_{\mathrm{L}}U_{\mathrm{Lf}}^2 \tag{12}$$

The friction factors f_{f} is evaluated as CRe_{L}^{-n} ($n=1$, $C=16$ for laminar flow and $n=0.2$, $C=0.046$ for turbulent flow). Carrying out the integration of Eqs. (10) or of Eqs. (11) up to a prescribed EB length, $\widetilde{L}_{\mathrm{B}}=L_{\mathrm{B}}/D$, yields the in situ gas fraction at the EB tail, $\varepsilon_{\mathrm{B}}^{\mathrm{w}}$ and the corresponding velocity in the liquid film:

$$U_{\mathrm{Lf}}^{\mathrm{w}}=\frac{U_{\mathrm{LS}}}{1-\varepsilon_{\mathrm{B}}^{\mathrm{w}}};\quad \varepsilon_{\mathrm{B}}^{\mathrm{w}}=1-\varepsilon_{\mathrm{f}}^{\mathrm{w}}\,|_{\tilde{z}=\widetilde{L}_{\mathrm{B}}} \tag{13}$$

For a long EB, the asymptotic fully developed film thickness $\tilde{\delta}$ (on $\tilde{h}$) corresponds to $\mathrm{d}\varepsilon_{\mathrm{f}}/\mathrm{d}\tilde{z}=0$, whereby the numerator of Eqs. (10) (or (11)) equals zero. In this case, the solution for $\tilde{\delta}$ can also be replaced by other models for the film thickness in an annular configuration. For instance, the Nusselt (1916) solution for a fully developed laminar falling film and the solution based on 1/7th power law velocity distribution for turbulent film flow (e.g. Brauner, 1987) can be applied:

$$\frac{\delta}{(\eta_{\mathrm{L}}^2/\rho_{\mathrm{L}}\Delta\rho g\sin\beta)^{1/3}}=0.909Re_{\mathrm{L}}^{1/3};\quad \text{laminar film} \tag{14.1}$$

$$\frac{\delta}{(\eta_{\mathrm{L}}^2/\rho_{\mathrm{L}}\Delta\rho g\sin\beta)^{1/3}}=0.135Re_{\mathrm{L}}^{7/12};\quad \text{turbulent film} \tag{14.2}$$

where $Re_{\mathrm{L}}=\rho_{\mathrm{L}}U_{\mathrm{LS}}D/\eta_{\mathrm{L}}$.

3. Solution procedure

The maximal gas supply rate for which unbounded bubble growth does not take place corresponds to the maximal bubble entrainment rate at the EB tail, associated with the maximal film velocity. The latter is obtained with a fully developed liquid film corresponding to $L_{\mathrm{B}}\to\infty$. In this case, the model requires a solution of four non-linear algebraic equations (NLE system) for the unknowns $\tilde{h}$ (or $\tilde{\delta}$), U_{GS}, $\varepsilon_{\mathrm{L}}^{\mathrm{w}}$ and $\varepsilon_{\mathrm{L}}^{\mathrm{s}}$. The four equations are the numerator of Eqs. (10) (or (11)) (8), (9.1) and (9.2) (all written as implicit equations with zero on their r.h.s.). The other model equations are explicit auxiliary equations that are needed for solving these four implicit equations. The solution so obtained yields the asymptotic values of the film thickness and velocity, δ^{∞} (or

h^{∞}) and U_{Lf}^{∞}, the maximal gas entrainment rate $U_{\mathrm{GS}}^{\infty}(\equiv \Phi_{\mathrm{GS}}^{\infty})$, the in situ void fraction in the EB wake and in the liquid flow downstream, $(\varepsilon_{\mathrm{L}}^{\mathrm{w}})^{\infty}$ and $(\varepsilon_{\mathrm{L}}^{\mathrm{s}})^{\infty}$, respectively. The NLE system has been solved using the POLYMATH software package (Shacham and Cutlip, 1996).

In case of developing EB and liquid film, the model requires integration of the differential equations (10) (or (11)) for the film thickness up to a specified length $\tilde{z} = \widetilde{L}_{\mathrm{B}}$. For a short EB, for which $We < We_{\mathrm{c}}$ (see (2)), gas is not entrained into the liquid, hence $\Phi_{\mathrm{GS}} = U_{\mathrm{GS}} = 0$.

For $We > We_{\mathrm{c}}$, the integration of the differential equation is coupled with implicit algebraic equations for $\varepsilon_{\mathrm{L}}^{\mathrm{w}}$ and $\varepsilon_{\mathrm{L}}^{\mathrm{s}}$ (Eqs. (9)), and for U_{GS}. Therefore, for a finite L_{B}, the solution requires integration of a differential algebraic equations (DAE) system. For this purpose, the controlled integration algorithm (Shacham et al., 1996) for converting the DAE into an ordinary differential equation (ODE) system has been applied. Alternatively, the gas entrainment rate in case of undeveloped film can be calculated by replacing the momentum equation (10) (or (11)) by a prescribed value of liquid film holdup at the bubble tail, $\varepsilon_{\mathrm{f}}^{\mathrm{w}}$. The prescribed value should be in the range $\varepsilon_{\mathrm{f}}^{\mathrm{w}}(\tilde{z} \to \infty) < \varepsilon_{\mathrm{f}}^{\mathrm{w}} < \varepsilon_{\mathrm{f}}(\tilde{z} = 0)$. The remaining three algebraic equations are solved to obtain U_{GS}, $\varepsilon_{\mathrm{L}}^{\mathrm{w}}$, $\varepsilon_{\mathrm{L}}^{\mathrm{s}}$. Then, the corresponding EB length, can be obtained by integrating Eqs. (10) (or (11)) up to the prescribed value of ε_{f}.

4. Discussion

To examine the TBW model for gas entrainment from stationary elongated bubbles, the model predictions are compared with experimental data available from the literature. However, the application of the drift flux model requires assigning values for the distribution parameters C_0^{w} and C_0^{s}, which account for the different bubble concentration and velocity profiles in the EB near and far wake regions.

In fully developed pipe flow, wall peaking in bubbles concentration generally results in $C_0 < 1$, whereas $C_0 > 1$ characterizes core peaking (see the discussion in Section 3 in Part A, Brauner and Ullmann, 2004). In case of vertical systems, downstream the EB wake region, where a fully developed bubbly flow is established, core-peaking of bubbles is typically observed. Therefore, $C_0^{\mathrm{s}} \geqslant 1$ is used. In inclined tubes and low liquid flow rates, the entrained bubbles tend to segregate due to buoyancy. In this case $C_0^{\mathrm{s}} < 1$ may represent bubbles peaking at the upper tube wall.

In the EB near wake region the flow is more complex and the appropriate distribution coefficient is essentially unknown. Here, due to the penetrating liquid film, the maximal downward velocity is located near the tube wall. Hence, the bubbles in the wake core are experiencing lower downward velocity (or even upward velocity). In this case, $C_0^{\mathrm{w}} < 1$ characterizes core peaking of bubbles. Note that $C_0^{\mathrm{w}} > U_0^{\mathrm{w}}/U_{\mathrm{m}}$ is required to represent downward shedding of bubbles at steady conditions (see Eq. (5.1)). It is further of interest to note that in contrast to the case of stationary EB, in slug flow $C_0^{\mathrm{w}} > 1$ represents core peaking of bubbles in the Taylor bubble wake.

Fig. 2 shows the results obtained for the case where an elongated bubble is formed in downward water flow in a pipe inclined by 30° to the horizontal. The experimental data have been reported by Hernandez-Gomez and Fabre (2001) and include the gas injection flux, U_{GS} as function of the stable elongated bubble length. Motivated by the problem of gas entrainment in slug flow, the liquid flow rate in their experiment was set at the value required to maintain the long bubble stationary in the liquid down-flow, $U_{\mathrm{LS}} = 0.57$ m/s. Using the Nicklin et al. (1962) equation for

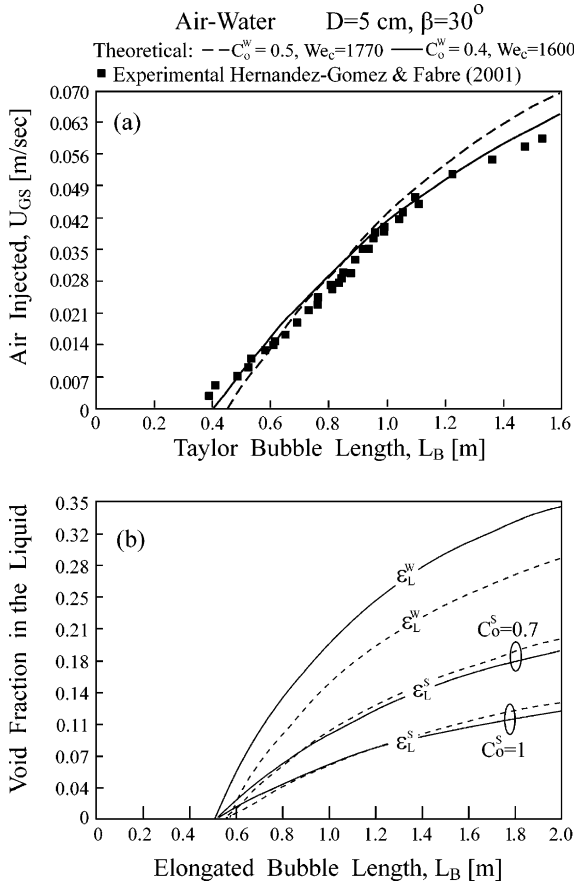

Fig. 2. The relation between the EB length and the air entrainment from its tail in a 30° inclined tube—comparison with the data of Hernandez-Gomez and Fabre (2001).

representing the bubble motion, $U_T = C_0^{TB} U_{LS} - U_0^{TB} = 0$, and the measured value of the bubble drift (U_0^{TB}), they noted that the associated distribution parameter, $C_0^{TB} (= U_0^{TB}/U_{LS})$ is about 0.7. It is worth noting that $C_0 < 1$ is in agreement with other experimental studies in countercurrent inclined flows (e.g. Nicklin et al., 1962; Bendiksen, 1984). Following the above discussion on the distribution parameters, even lower values of C_0^w may be required to characterize the bubble flow in the EB wake.

Fig. 2a shows a comparison of the predicted gas injection rate with the experimental data. Air entrainment from the EB tail is initiated only when its length exceeds a threshold value, $(L_B)_{crit}$. Therefore, in the range of $0 < L_B < (L_B)_{crit}$, once the EB is formed, its length can be maintained without gas injection. The model attributes the critical bubble length to a critical Weber number, which corresponds to a critical velocity difference between the liquid in the film and in the EB wake. As shown in the figure, the critical Weber number (Eq. (1)) predicts the critical EB length for the onset of entrainment (8–9*D*). For $L_B > (L_B)_{crit}$, a continuous injection of air is required in order to compensate for the gas entrainment rate at the EB tail. A longer EB results in a higher

velocity in the film, hence, higher rate of gas entrainment from the EB. Therefore, higher U_{GS} is required for maintaining that EB length. The model follows the trend of increasing U_{GS} with L_B, approaching the maximal entrainment rate, which corresponds to a fully developed liquid film flow at the tail of a long EB. However, for the longest EB used in the experiment ($L_B \simeq 1.6$ m), the slope of the curve implies that the maximal entrainment rate has not yet been achieved.

Fig. 2a demonstrates that the rather small discrepancy between the model predictions and the data can be attributed to some variation in the model parameters, such as the critical Weber number and the distribution parameter. A lower value of C_0^w reduces the downstream velocity of the entrained bubbles, resulting in a higher liquid velocity (see Eqs. (5)). Since the film and liquid in the wake flow concurrently, a lower value of C_0^w results in a lower bubble entrainment rate. It is worth noting, that this is in contrast to slug flow, where higher values of C_0^w affects lower entrainment rate (see Part A, Brauner and Ullmann, 2004). In slug flow, however, the film plunges into a countercurrent liquid flow. This is an essential difference between real slug flow and its simulation as attempted by experiments with stationary EB's.

Fig. 2b shows the predicted gas fraction entrained into the liquid stream. The void fraction of the entrained bubbles increases with the bubble length, with $\varepsilon_L^w \simeq 0.3$ predicted for the longest bubble used in the experiments. If $C_0^s = C_0^w$ is assumed, the bubble velocities, as well as the void fraction are the same in the near and far EB wake regions. Otherwise, if the fully developed bubbly flow established in the far wake region corresponds to $C_0^s > C_0^w$, then the gas fraction in the near EB wake region, ε_L^w is higher than in the far wake region downstream, ε_L^s.

Fig. 3 demonstrates the results obtained in case a stationary EB is injected into liquid down-flow in a vertical pipe. The pipe diameter of 9.97 cm is that used by Delfos et al. (2001a) and the model predictions are compared with their experimental data. The data include the gas injection rate vs. the EB length, as well as the resulting average gas fraction downstream the liquid column, $\overline{\varepsilon}_L^s$. The experiments were carried out for three water flow rates, corresponding to $Fr_{TB} = U_{LS}/U_0^{TB} = 1, 1.2$ and 1.4. Delfos et al. (2001a) also showed curve fits of the drift flux model to represent the variation of the measured (average) $\overline{\varepsilon}_L^s$ with the gas injection rate. These fits indicated a decreasing value for the average distribution parameter, $\overline{C}_0$ with increasing the liquid flow rate ($\overline{C}_0 \simeq 1.07$ to $\overline{C}_0 = 1.027$ with Fr_{TB} increasing from 1 to 1.4). Accordingly, the TBW model is applied with $C_0^s = 1.05$. In view of the above physical arguments, a lower value of the distribution parameter is used for the wake region. The results in Fig. 3a–c were obtained with $C_0^w = 0.8$ for all three flow rates. Although the results shown in these figures indicate a favorable comparison with the data, even a better fit can be obtained with some tuning of C_0^w ($= 0.9, 0.7, 0.65$ for $Fr_{TB} = 1, 1.2, 1.4$ respectively in Fig. 3d–f). A trend of decreasing C_0^w with the liquid flow rate is also consistent with that indicated by the above averaged reported $\overline{C}_0$ values. Such a trend can be expected, as higher liquid flow rate results in a higher momentum of the penetrating film, and thus a more distorted velocity profile in the EB wake region.

Albeit the different flow configuration at the EB region, the bubble entrainment phenomenon in the vertical column is in principle similar to that obtained in the inclined column. The gas loss due to the bubble entrainment increases with the bubble length, once it is longer than the critical length for the onset of entrainment. The data and the model imply a critical bubble length of about $2D$, which is lower than that obtained in the inclined column. This is due to the higher film velocity at the steeper inclinations and a larger tube diameter. Both the model and the data indicate that the asymptotic gas entrainment (corresponding to a long EB) is practically

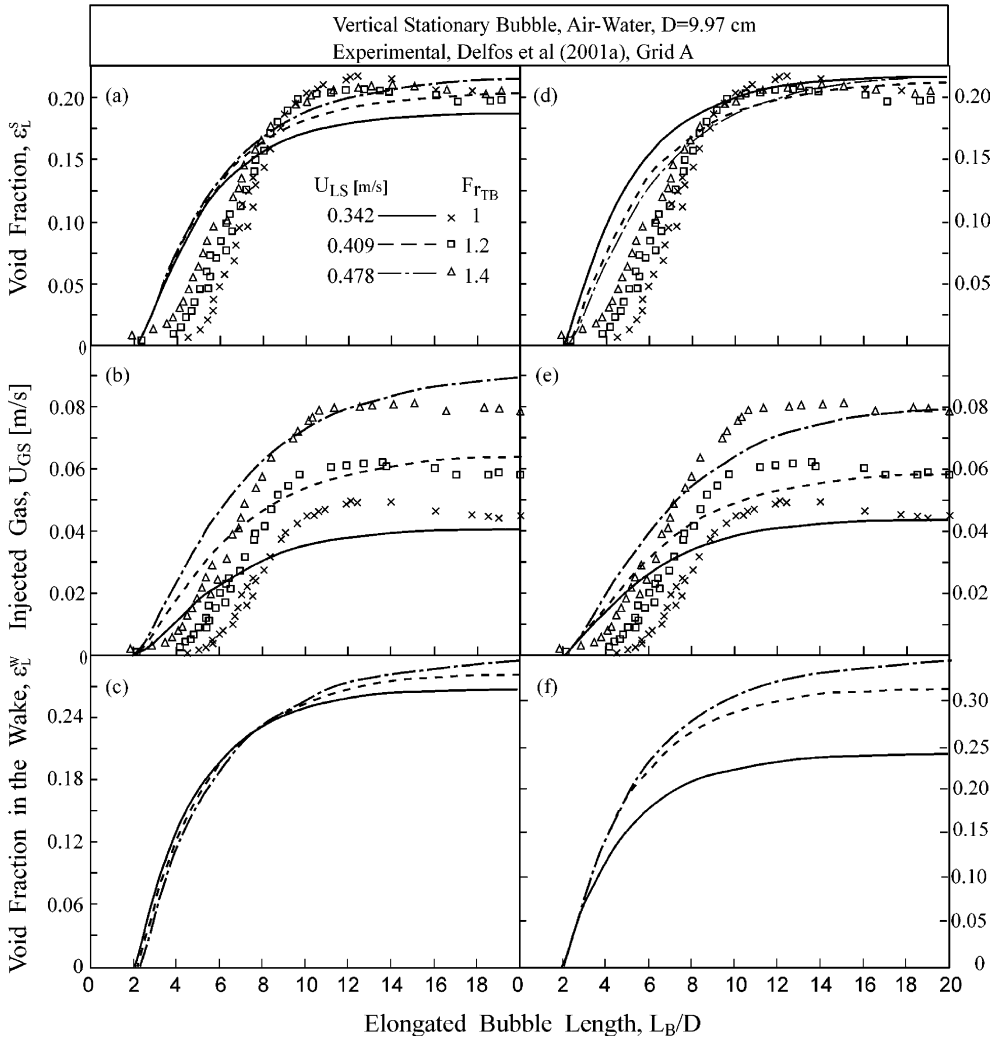

Fig. 3. The effect of the water flow rate and the EB length on air entrainment in a vertical column—comparison with the data of Delfos et al. (2001a): (a, d) downstream void fraction, (b, e) rate of entrained air, (c, f) void function in the wake. $C_0^s = 1.05$; In (a–c) $C_0^w = 0.8$. In (d–f) $C_0^w = 0.9$, 0.7, 0.65 for $Fr_{TB} = 1$, 1.2, 1.4 respectively.

approached already with a bubble length of about 20D. However, an exact fit of the model with the data could not be expected with the rather simplistic one-dimensional model which is used to represent the EB shape, in particular for relatively short EB's. It is to be noted that the data imply a maximal gas entrainment rate at $L_B \simeq 12D$, which is not predicted by the model. However, in the other experimental studies (cited in the introduction section) such a maximum has not been reported. A maximum in gas loss may be a result of variations of the flow field in the EB wake at higher film velocities associated with the longer EB's. These can be represented in the model by declining values of C_0^w. Consequently, the increase of the back-flow (Φ_{Gb}) with the EB length may be steeper than that of Φ_{Ge}, which may then result in a maximal net gas entrainment at a certain

bubble length. It is worth emphasizing that the back-flow predicted by the model in case of a stationary EB is very significant. About 50% of the entrained bubbles are recycled back to the EB tail. This is supported by experimental findings recently reported by Delfos et al. (2001b).

Consistent with the data, the model predicts that the bubble void fraction downstream the EB saturates at $\varepsilon_L^s \simeq 0.2$ (Fig. 3d). Although, the rate of gas entrainment increases with the liquid flow rate (Fig. 3e), ε_L^s is insensitive to the water rate. However, the void fraction at the EB wake region, ε_L^w is predicted to increase with the water flow rate (Fig. 3f). It reaches a value of 0.25 for $Fr_{TB} = 1$ and about 0.35 for $Fr_{TB} = 1.4$. Delfos et al. (2001a) did not measure the local void fraction, but provide photographs of the EB wake region. These photographs show a highly aerated wake region adjacent to the EB tail of about 1–1.5D long, in particular for $Fr_{TB} = 1.2$ and 1.4.

Delfos et al. (2001a) also used two different grids (denoted by A and B) to regulate the turbulence level upstream the EB. Their data shown in Fig. 3 have been obtained with grid A. The additional grid B was used to enhance the turbulence level in the water flow, and the corresponding data is shown in Fig. 4. The enhanced turbulence results in a lower critical EB length. For this case, a better agreement between the model predictions and the data for short EB's is obtained when the We_c is reduced by about 50% ($C' = 0.33$ in Eq. (2.2)). This implies that for a relatively short EB, the turbulence intensity in the wake is affected also by the turbulence in the

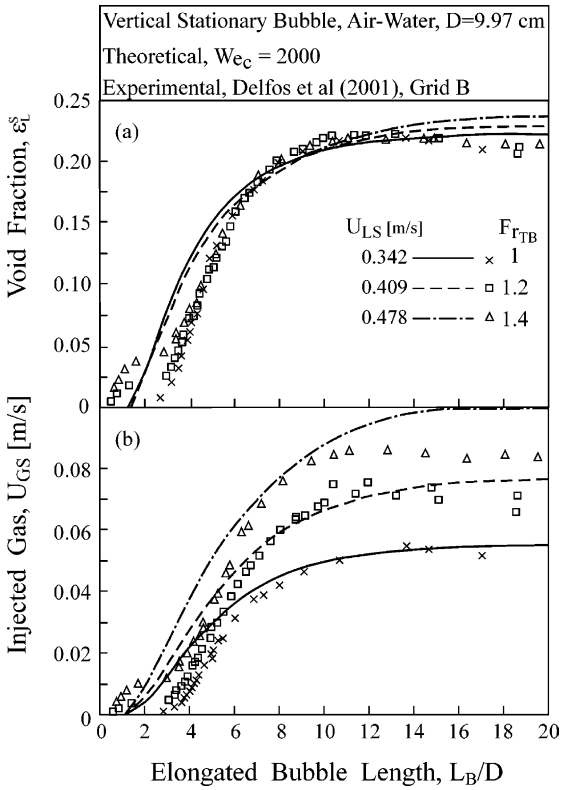

Fig. 4. Comparison of the model predictions with the data of Delfos et al. (2001a) in enhanced turbulent flow for $We_c = 2000$. $C_0^s = 1.05$; $C_0^w = 0.9$, 0.7, 0.65 for $Fr_{TB} = 1$, 1.2, 1.4 respectively.

liquid flow approaching its nose. In any case, the effect of We_c on the predictions diminishes for high film velocities corresponding to longer EB's and/or higher flow rates.

Data on the rate of gas entrainment from stationary large bubbles attached to spargers in vertical downcomers were reported by Bacon et al. (1995a,b) and Lee et al. (1997, 1999). Comparison of the model predictions with these data is more problematic, as the rate of air entrainment was found to be dependent on the structure of the sparger (horizontal, central or peripheral). Evidently, the associated bubble shape is not expected to follow the model, which corresponds to a 'free' EB. This limitation is probably more significant for relatively short bubbles; for a long EB, the characteristics of the fully developed film are expected to be insensitive to the upstream boundary conditions. Therefore, the model should be appropriate for the prediction of the entrainment rate associated with the long EB's in those experiments. The longest EB's were limited by the height of the downcomer and are of about $20D$ for the two tube diameters used in the experiments ($L_B \simeq 1.2$, 2 m for $D = 5.6$, 10.5 cm, respectively). Therefore, the apparent maximal entrainment rate data is compared with the model predictions for $L_B = 20D$.

Fig. 5 shows a comparison of the predicted air entrainment rate vs. the film velocity in comparison with the data obtained by Bacon et al. (1995b) and Lee et al. (1997) with glycerol solution and the horizontal (HS) sparger. These coordinates were used by Lee et al. (1999) following the suggestion of Sene (1988). However, scaling the entrainment rate by the width of the jet could not remove the diameter effect. The model confirms that even with such a scaling, the rate of air entrainment increases with the tube diameter. The predicted values are shown for $C_0^w = 0.8 \div 1$ with $We_c \neq 0$ and $C_0^w = 1$ with $We_c = 0$. In accordance with the comparison with Delfos et al. (2001a) data, the distribution parameter C_0^w for the bubbly flow in the EB wake seems to decrease with the larger film velocity obtained at higher liquid flow rates. The value of $C_0^w \simeq 1$, which is used at low velocities, may seem unrealistic. However, with a lower We_c, the data at low flow rates

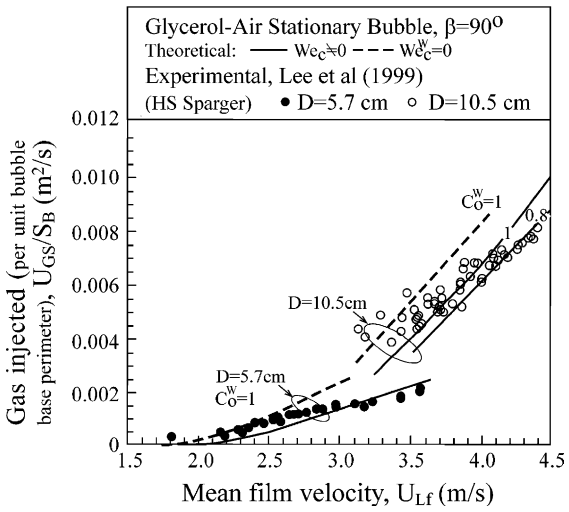

Fig. 5. Effect of tube diameter and the film velocity on the rate of air entrainment from a stationary EB in vertical down-flow of glycerol solution—comparison of the model prediction for $L_B = 20D$ with the data shown in Lee et al. (1999) for a horizontal sparger.

can be explained with lower values of C_0^w. Indeed, the data reported in those studies for the entrainment rate vs. the bubble length, indicate a much shorter critical length than that implied by the We_c used in the model (with $C' = 0.66$ in (2)). This may be a result of the turbulence induced in the flow due to the sparger. It is expected to be more significant with relatively short EB, where the film flow and turbulence in the wake may be largely affected by the upstream flow field. At relatively low liquid flow rates of Fig. 5, 'run away' conditions were obtained with relatively short EB's, whereby the upstream turbulence may be influential. For high film velocities (high liquid flow rates), the effect of the We_c is modest.

Similar conclusions can be drawn in view of the comparison of the model predictions with the data of Lee et al. (1997) and Bacon et al. (1995a,b) for water–air system (Fig. 6a and b) and for propanol–air system (Fig. 6c). While glycerol was used in the experiments to study the effect of the liquid viscosity (7–9 times higher than that of water but was the same surface tension), the use of propanol was to evaluate the effect of surface tension (near half of that of water, while $\eta_L = 2\eta_w$).

By dimensional analysis, Lee et al. (1997, 1999) identified the liquid Froude number, $Fr_L = \frac{\pi}{4}\frac{U_{LS}}{\sqrt{gD}}$, the viscosity number $N_\eta = \eta_L/(\rho_L\sqrt{gD^3})$ and the Eotvös number (Eo_D) as the relevant dimensionless groups that control the dimensionless maximal gas entrainment rate. The latter was represented by the gas Froude number, $Fr_G = \frac{\pi}{4}\frac{U_{GS}}{\sqrt{gD}}$. Experimental correlations have been suggested that indicate that the data obtained with a particular sparger can be represented by $Fr_G\,Eo^{-0.5}N_\eta^m = f(Fr_L)$ with $m < 0.1$. Thus, the N_η effect is practically insignificant (in view of the 95% confidence interval reported for the parameter m). It is of particular interest here to examine whether a similar correlation evolves from the TBW model.

To that aim, the model equations are simplified by ignoring the drift between the entrained bubbles and the liquid ($U_G^w \simeq U_L^w \simeq U_m$), suppressing the back-flow and assuming $U_{GS} \ll U_{LS}$, $We_c = 0$, and $\tilde{\delta} \ll 1$. As the maximal entrainment rate is obtained with a fully developed film flow,

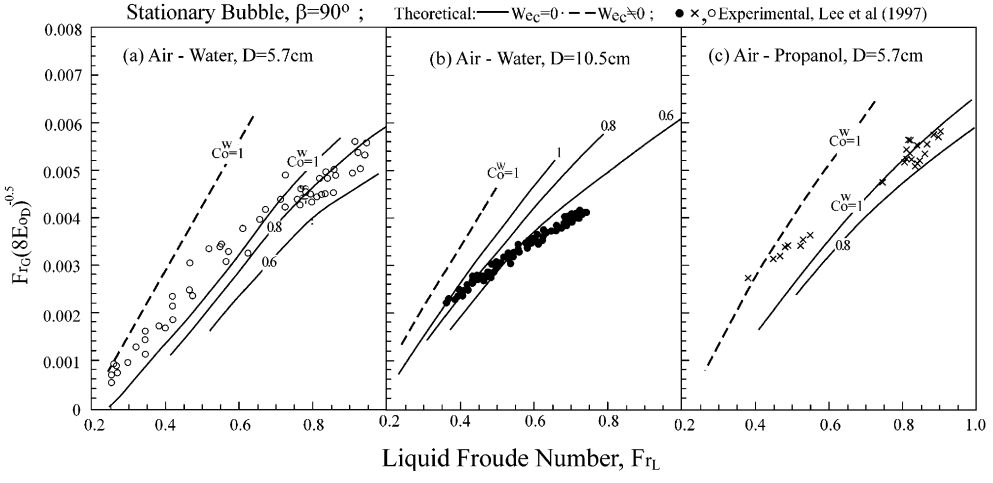

Fig. 6. Effect of down-flow rate on air entrainment from an EB in a vertical tube—comparison of the model prediction for $L_B = 20D$ with the data shown in Lee et al. (1997) for a horizontal sparger: (a) water down-flow $D = 5.7$ cm, (b) water down-flow $D = 10.5$ cm, (c) propanol down-flow $D = 5.7$ cm.

Eq. (14.1) for laminar flow or Eq. (14.2) for a turbulent film are used. These lead to the following equations (only linear terms of $\tilde{\delta}$ are retained):

$$Fr_{\mathrm{G}}\,Eo_D^{-1/2}N_\eta^{1/6}\left(\frac{\Delta\rho}{\rho_{\mathrm{L}}}\right)^{1/3}=A_1^{\mathrm{T}}\,Fr_{\mathrm{L}}^{11/6}\left[1-A_2^{\mathrm{T}}\left(\frac{\Delta\rho}{\rho_{\mathrm{L}}}\right)^{-1/3}N_\eta^{1/12}\,Fr_{\mathrm{L}}^{7/12}\right];\quad\text{turbulent film}\tag{15.1}$$

$$Fr_{\mathrm{G}}\,Eo_D^{-1/2}N_\eta^{2/3}\left(\frac{\Delta\rho}{\rho_{\mathrm{L}}}\right)^{5/3}=A_1^{\mathrm{L}}\,Fr_{\mathrm{L}}^{7/3}\left[1-A_2^{\mathrm{L}}\left(\frac{\Delta\rho}{\rho_{\mathrm{L}}}\right)^{-1/3}N_\eta^{1/3}\,Fr_{\mathrm{L}}^{1/3}\right];\quad\text{laminar film}\tag{15.2}$$

where $A_1^{\mathrm{T,L}}$ and $A_2^{\mathrm{T,L}}$ are numeric constants (the term on the r.h.s. brackets represent $(1-7\tilde{\delta})$).

Not surprisingly, practically the same dimensionless groups are implied by the model ($\Delta\rho/\rho_{\mathrm{L}}\simeq 1$ for the low pressure air–liquid systems used in the experiments). However, the same exponent of Eo_D indicated by the model and by the correlation, as well as the mild dependence on $N\eta$ (in case of turbulent flow, as in the experiments), further substantiate the validity of the model assumptions. It is worth recalling that the scaling of U_{GS} as proportional to $\sigma^{-0.5}$ evolves in the model from the combined effect of the Weber number and $\tilde{d}_{\mathrm{crit}}$. Incidentally, the model suggests the following alternative dimensionless representation of Eqs. (15):

$$\left(\frac{U_{\mathrm{GS}}}{U_{\mathrm{LS}}}\right)Eo_D^{-1/2}\left(N'_\eta\right)^{-1/3}=A_{1'}^{\mathrm{T}}\,Re_{\mathrm{L}}^{5/6}[1-A_{2'}^{\mathrm{T}}(N'_\eta)^{1/3}\,Re_{\mathrm{L}}^{7/12}];\quad\text{turbulent film}\tag{16.1}$$

$$\left(\frac{U_{\mathrm{GS}}}{U_{\mathrm{LS}}}\right)Eo_D^{-1/2}(N'_\eta)^{-1/3}=A_{1'}^{\mathrm{L}}\,Re_{\mathrm{L}}^{4/3}[1-A_{2'}^{\mathrm{L}}(N'_\eta)^{1/3}\,Re_{\mathrm{L}}^{1/3}];\quad\text{laminar film}\tag{16.2}$$

where $N'_\eta=\eta_{\mathrm{L}}^2/(\rho_{\mathrm{L}}\,\Delta\rho g D^3)$. This form pinpoints the liquid Reynolds number, rather than the Froude number as a controlling dimensionless group, and the $\Delta\rho/\rho_{\mathrm{L}}$ term is embedded in the viscosity number. Obviously, the same weak dependence on the liquid viscosity is implied by these two forms of the model for turbulent flow in the film. However, for laminar film flow, the effect of the liquid viscosity is predicted to be much more significant. It is worth noting, however, that the liquid viscosity may have an additional effect on the critical bubble size, which has not yet included in Eqs. (3). A viscosity effect is expected only in highly viscous liquids (see the map of bubbles/drops shape regimes in Clift et al., 1978).

The increase of the maximal rate of gas entrainment with the liquid flow rate as implied by Eqs. (15) or (16) is steeper than the linear dependence suggested by Lee et al. (1999) correlation. This maybe a result of the underlying simplifying assumptions (listed above) that have been used to derive these equations. As shown in Figs. 5 and 6, the full model is capable of following the trend indicated by the data. However, some concern should be raised regarding the data. The values reported as the maximal gas entrainment rate were actually not measured directly. The procedure used for deducing the maximal gas rate is described in Bacon et al. (1995a,b): "The air flow rate was increased to a value that would cause the bubble to expand, continuously and slowly. The time (Δt) taken for the bubble length to increase by a measured distance (Δz) was recorded and the rate of increase in the bubble volume was calculated via use of a correlation for the liquid thickness. This rate of increase of bubble volume was taken to be the difference between the maximum entrainment (U_{GS}^{∞}) and the rate of supply of air to the sparger ($U_{\mathrm{GS}}^{\mathrm{exp}}$)". This means that the following equation was used:

$$\Delta U_{GS} = U_{GS}^{exp} - U_{GS}^{\infty} = \left(\frac{\Delta z}{\Delta t}\right)_{exp} \varepsilon_B^{\infty} \tag{17}$$

However, when expanding bubble is encountered, the extra rate of gas feed which is required to compensate for the increase of the bubble volume is actually given by

$$\Delta U_{GS} = \frac{\Delta z}{\Delta t}(\varepsilon_B^w - \varepsilon_L^w) \tag{18}$$

The gas fraction in the EB wake, ε_L^w was not measured and not included in the correction term. Moreover, $\varepsilon_B^w (< \varepsilon_B^{\infty})$ may be required to represent the void fraction of the finite length EB. Consequently, the reported data for the maximal entrainment rate may underpredict the real maximal values. The deviation is expected to become more significant with increasing the liquid down-flow, as the EB wake region becomes highly aerated and longer EB are required to approach the asymptotic value, ε_B^{∞}. However, since the data of $(\Delta z/\Delta t)_{exp}$ were not reported, the corrections suggested by Eq. (18) could not be included in the comparison of the model predictions with these data.

5. Conclusions—implications to slug flow

The underlying physical mechanism for the gas entrainment either from a stationary elongated bubble, or from a Taylor bubble in slug flow, are essentially the same. The rate of gas entrainment from the bubble tail is determined by the rate of turbulent kinetic energy available at the bubble wake for recurrent generation of the surface energy of the entrained bubbles. Although the shape of a stationary EB depends on the type of the injection nozzle being used and may differ from the shape of a free TB, the differences are expected to have a dominant effect only for relatively short EB's. For a long EB, the flow in the liquid film approaches the fully developed characteristics and the effect of the upstream conditions diminishes.

The main difference between gas entrainment from a stationary EB and a rising TB bubble (as in upward slug flow) is the direction of the film velocity relative to the liquid flow in the EB wake. In case of a stationary EB, the liquid film penetrates concurrently a down-flowing liquid. Whereas in slug flow, the liquid film plunges into a countercurrent up-flow of liquid in the slug. Hence, the intensity of the turbulence in the shear layer, which is responsible for the EB fragmentation, is not the same. Also, in slug flow bubble back-flow is suppressed as the TB drift velocity is higher than that of the bubbles in the swarm formed at its wake. Whereas with a stationary EB, a significant back-flow is predicted. It is, therefore, of interest to evaluate the effect of these inherent differences on the rate of gas entrainment and the resulting void fraction in the liquid for these two cases.

For a Taylor bubble rising through un-aerated liquid flowing upward at a rate U_m, the rise of velocity is expressed by Nicklin et al. (1962) equation, $U_T = C_0^{TB} U_m + U_0^{TB}$. A stationary TB is viewed in a coordinate system, which is attached to the rising TB, whereby the apparent downward liquid flow rate is $U_{LS} = U_T - U_m$. Therefore, when a simulation of slug flow is of concern, the following relation between the up-flow velocity in the slug (U_m) and the liquid down-flow (U_{LS}) is used (Delfos et al., 2001a):

$$U_{\mathrm{m}} = \frac{U_{\mathrm{LS}} - U_0^{\mathrm{TB}}}{(C_0^{\mathrm{TB}} - 1)} \tag{19}$$

where U_0^{TB} is the TB drift velocity (see Eq. (10) in Part A, Brauner and Ullmann, 2004).

Fig. 7 shows the results obtained by applying the TBW model to upward air-water slug flow in a vertical tube of $D = 9.97$ cm, and the U_{m} corresponding to liquid down-flow of $U_{\mathrm{LS}} = 0.409$ m/s. This is one of the flow rates used in Delfos et al. (2001a) experimental study on entrainment from a stationary TB and was studied in Fig. 3. Fig. 7a shows the rate of gas entrainment from an upward moving TB. The void fraction at the wake, $\varepsilon_{\mathrm{LS}}^{\mathrm{w}}$ and in the slug, $\varepsilon_{\mathrm{LS}}^{\mathrm{s}}$ are shown in Fig. 7b. The results were obtained with $C_0^{\mathrm{s}} = 1.05$ (the same value used for a stationary EB in Fig. 3) and $C_0^{\mathrm{w}} = 1.05$–1.2 to represent the core peaking of the (upward) velocity in the TB wake. A detailed discussion on the effects of these model parameters on the predicted values has been presented in Part A of this study (Brauner and Ullmann, 2004). However, as shown in Fig. 7, the variations with the value used for C_0^{w} are modest. In case of the $D \sim 10$ cm tube, bubble back-flow is not likely in view of the large TB drift velocity ($\Phi_{\mathrm{Gb}} = 0$ via Eq. (13) in Part A). Comparison of Figs. 7a and 3a indicates that for a rising TB, the entrainment rate is 2–3 times larger then that obtained in the corresponding case of a stationary TB. The moving TB wake region is much more aerated, and $\varepsilon_{\mathrm{LS}}^{\mathrm{s}}$ ($= 0.35$–0.4) is 1.5–2 times higher compared to the $\varepsilon_{\mathrm{L}}^{\mathrm{s}} = 0.2$ value in Fig. 3b. It is worth recalling, that with $C_0^{\mathrm{s}} = C_0^{w}$, $\varepsilon_{\mathrm{LS}}^{\mathrm{s}} = \varepsilon_{\mathrm{LS}}^{\mathrm{w}}$ is predicted, implying even more aerated slugs. Similarly to the stationary TB, also with the rising TB, the maximal entrainment rate is practically approached already for $L_{\mathrm{B}} \simeq 20D$.

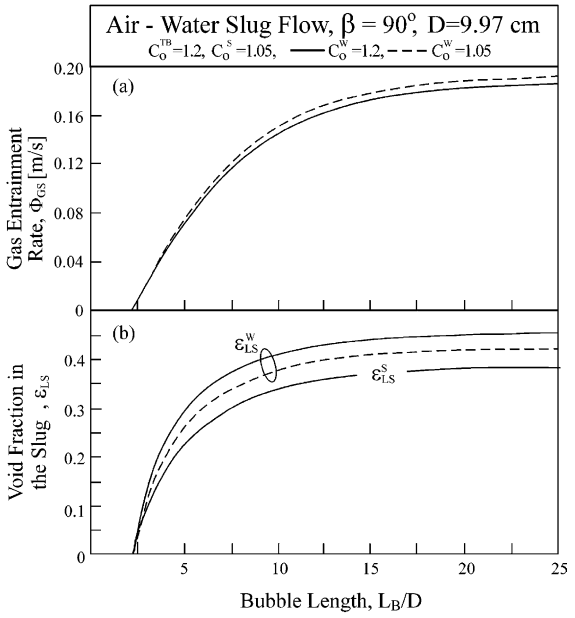

Fig. 7. Air entrainment from a rising Taylor bubble corresponding to $U_{\mathrm{LS}} = 0.409$ m/s in Fig. 3—effects of model parameters on the prediction: (a) rate of entrained gas, (b) void fraction in the TB wake, $\varepsilon_{\mathrm{LS}}^{\mathrm{w}}$ and in the liquid slug, $\varepsilon_{\mathrm{LS}}^{\mathrm{s}}$.

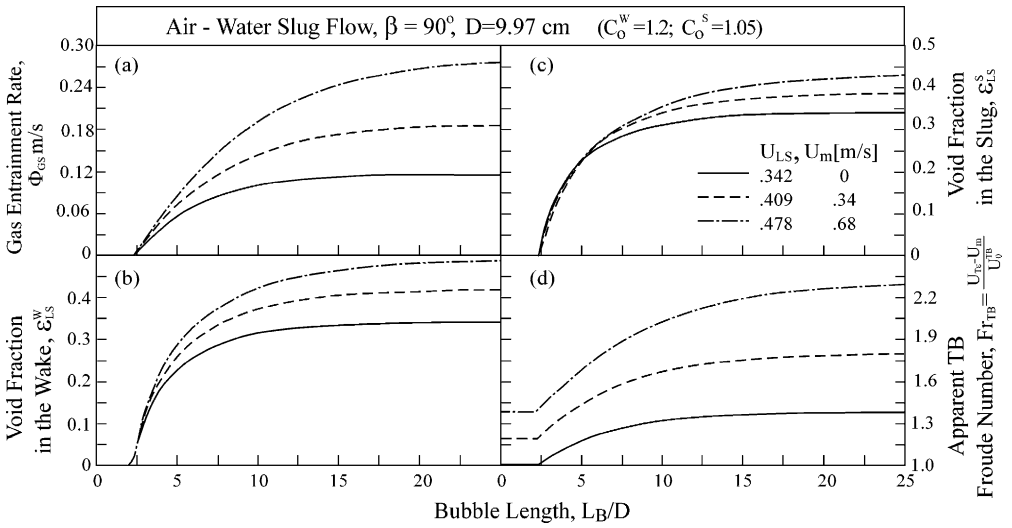

Fig. 8. Air entrainment from a rising TB corresponding to the three flow rates used in Fig. 3: (a) rate of gas entrainment, (b) void fraction in the TB wake, (c) void fraction in the liquid slug, (d) dimensionless apparent TB translational velocity.

The same conclusions are drawn in view of the comparison between Fig. 8 (moving TB) and Fig. 3 (stationary TB) for the three flow rates for which the down-flow experiments were conducted. The entrainment rate from a rising TB is much higher, and consequently the liquid slug is much more aerated. It is worth recalling here, that in the case of a rising TB as in slug flow, the apparent TB translational velocity, $U_{T\varepsilon}$ is higher than that predicted by Nicklin et al. (1962) equation, U_T. This is due to the recurrent coalescence of bubbles with the TB nose and the simultaneous re-entrainment at its tail resulting in an additional apparent bubble drift. In case the liquid ahead of the TB is un-aerated, the TB becomes shorter while moving upward, whereby the apparent velocity of its tail is higher than that of its nose.

The apparent TB translational velocity (corresponding to the results shown in Fig. 8a–c) is shown in Fig. 8d. The scaling used $Fr_{TB} = (U_{T\epsilon} - U_m)/U_0^{TB}$ is that used by Delfos et al. (2001a) and corresponds to the dimensionless liquid down-flow as is viewed in the coordinate system attached to the TB in aerated slug. As shown, the apparent liquid down-flow increases with the bubble length due to the enhanced gas entrainment rate associated with longer TB's.

References

Bacon, R.P., Scott, D.M., Thorpe, R.B., 1995a. Large bubbles attached to spargers in downwards two-phase flow. Int. J. Multiphase Flow 21, 949–959.

Bacon, R.P., Scott, D.M., Thorpe, R.B., 1995b. Large bubbles in downward two-phase flow. Chem. Eng. Res. Des. 73A, 228–233.

Bendiksen, K.H., 1984. An experimental investigation of the motion of the long bubbles in inclined tubes. Int. J. Multiphase Flow 10, 467–483.

Brauner, N., 1987. Roll wave celerity and average film thickness in turbulent wavy film flow. Chem. Eng. Sci. 42, 265–273.

Brauner, N., Ullmann, A., 2004. Modelling of gas entrainment from Taylor bubbles. Part A: Slug flow. Int. J. Multiphase Flow 30, doi:10.1016/j.ijmultiphaseflow.2003.11.007.

Clift, R., Grace, J.R., Weber, M.E., 1978. Bubbles, Drops and Particles. Academic Press.

Delfos, R., Wisse, C.J., Oliemans, R.V.A., 2001a. Measurement of air entrainment from a stationary bubble in a vertical tube. Int. J. Multiphase Flow 27, 1769–1787.

Delfos, R., Rops, C.M., Kockx, J.P., Nieuwstadt, T.M., 2001b. Measurement of recoalescence flux into the rear of a Taylor bubble. Phys. Fluids Flow 13, 1141–1150.

Hernandez-Gomez, A., Fabre, J., 2001. An experimental study of the hydrodynamics of a stationary air–water slug. In: Proceedings of the ICMF 2001, 4th International Conference on Multiphase Flow.

Lee, Y.H., Scott, D.M., Thorpe, R.B., 1997. The scale-up of large bubbles attached to spargers in downward two-phase flow. Chem. Eng. Sci. 52, 3797–3809.

Lee, Y.H., Scott, D.M., Thorpe, R.B., 1999. The scale-up of large bubbles attached to spargers in downward two-phase flow. Chem. Eng. Sci. 54, 3839–3898.

Nicklin, D.J., Wilkes, J.O., Davidson, J.F., 1962. Two phase flow in vertical tubes. Trans. Int. Chem. Eng. 40, 61–68.

Nusselt, W., 1916. Surface condensation of water. Z. Ver de Ing. 60 (27), 541–546 (60 (26), 569–575).

Riiser, K., Fabre, J., Suzanne, C., 1992. Gas entrainment at the rear of a Taylor bubble. In: Proceedings of the European Two-Phase Flow Group Meeting, Stockholm, pp. 1–8.

Shacham, M., Cutlip, M.B., 1996. POLYMATH User's Manual, CACHE Corporation, Austin, TX.

Shacham, M., Brauner, N., Pozin, M., 1996. Application of feedback control principles for solving differential-algebraic systems of equations in process control education. Comput. Chem. Eng. 20, 1329–1334.

Sene, K.J., 1988. Air entrainment by plunging jets. Chem. Eng. Sci. 43, 2615–2623.